Simulation of solidification grain structures with a multiple diffusion length scales model

Salem Mosbah, Michel Bellet, Charles-André Gandin

Proc. MCWASP XII, 12th Int. Conf. on Modeling of Casting, Welding and Advanced Solidification Processes, Vancouver & Alaska, June 7-13, 2009, S. Cockcroft, D. Maijer (eds.), The Minerals, Metals & Materials Society, Warrendale, Pennsylvania, USA (2009) 485-493

SIMULATION OF SOLIDIFICATION GRAIN STRUCTURES WITH A MULTIPLE DIFFUSION LENGTH SCALES MODEL

S. Mosbah, M. Bellet, Ch.-A. Gandin

MINES ParisTech, CEMEF- Centre de Mise en Forme des Matériaux, CNRS UMR 7635,
BP 207, 1 rue Claude Daunesse, 06904 Sophia Antipolis Cedex, France

Keywords: Solidification, Structure, Segregation, Modeling

Abstract

A cellular automaton (CA) – finite element (FE) model is presented for the prediction of micro- and macrosegregation based on solute diffusion. On the one hand an open microsegregation model is implemented. It applies to each solidifying CA cell, i.e. a representative elementary volume of the mushy zone. Diffusion in the solid and in the extradendritic liquid are modeled with analytical expressions for two length scales based on the primary and secondary dendrite arm spacing and assuming cylindrical geometries representative of the dendritic network. On the other hand an unstructured and anisotropic FE mesh adaptation is used. The FE mesh is generated based on an error estimation method of the average composition field. Mesh refinement takes place in regions located ahead of the mushy zone growth front where diffusion layers are built up due to segregation. As a result, the diffusion length scale outside the envelopes of mushy zones (i.e., in the intergranular liquid that surrounds the envelopes of the grains) is directly captured. Numerical implementations of the coupling between the CA and FE methods being validated by comparison with the predictions of other models, simulations are compared with experimental results in Al-Cu alloys; thus demonstrating the capability of the model to predict segregation based on the coupling between several length scales.

Introduction

Detailed comparisons of modeling predictions with experimental observations of a single dendritic grain structure are rarely carried out. This is mainly due to little well defined experimental results as well as little casting technologies involving an isolated dendritic grain. For instance, single crystal production of nickel-base superalloys by directional solidification [1] and the atomization process of metallic alloys [2] could be seen as experimental models for a single columnar and equiaxed grains, respectively. Containerless techniques offer and advanced control of the nucleation of grains upon solidification. Indeed, the usual container walls in conventional casting, where nucleation is favored upon cooling, are suppressed. An example of such a technique is provided by the electromagnetic levitation (EML) of a volume of metallic alloy in the liquid and solid state. The melt can either cool down by heat exchange with the surrounding gas, in which case nucleation is referred to as "spontaneous", or by bringing a cooling device into contact with the sample, in which case nucleation is referred to as "triggered" [3, 4]. Because the size of the system is only a few cubic millimeters and close to the simple spherical geometry, it is perfectly suitable for advanced characterization and modeling. Recently, Gandin *et al*. [5, 6] used the EML technique to study the solidification of undercooled Al-Cu droplets, including the distribution of Cu, the interdendritic eutectic structure and the dendrite arm spacing (DAS). The thermal history could be recorded thanks to an optical pyrometer directed toward the top of the levitated sample surface. Data entering numerical modeling, such as the nucleation undercooling of the dendritic and eutectic microstructures, could be directly

measured. Predictions showed the importance of accounting for both the nucleation undercooling and the recalescence of the eutectic microstructure for retrieving the global volume fraction of phases averaged over the entire samples. However, the analysis was based on an extension of a simple uniform temperature model, assuming that an analytical expression for the solute diffusion length outside the envelope of the mushy zone could be deduced from a steady state approximation [7-9].
An extension of the more sophisticated two dimensional (2D) Cellular Automaton (CA) – Finite Element (FE) coupling approach [10-13] is presented hereafter for modeling both spontaneous and triggered EML samples. Diffusion in the liquid in front of the growing mushy zone is calculated through a direct numerical solution of the diffusion field by solving the average solute mass conservation equation with a refined FE mesh, while diffusion in the solid phase is accounted for in the microsegregation model applying at each CA cell. Predicted cooling curves are compared with measurements for spontaneous [5] and triggered Al-Cu samples, demonstrating the capability of the model to treat both situations where cooling and heating take place concomitantly to dendritic growth, typical of the columnar and equiaxed structures, respectively.

Experimental

Spherical Al-Cu binary alloy systems were processed by EML. Samples, with typically 0.2 g in mass, were prepared from pure Al (99.9999 %) and Cu (99.999 %). Compositions were selected as 4, 14 and 24 wt% Cu. The metal consisted of an approximately spherical volume with a diameter close to 5.3 mm containing a dendritic microstructure due to primary solidification from the melt and a eutectic microstructure resulting from secondary interdendritic solidification. Samples with the same alloy compositions were either spontaneously solidified or triggered with an alumina plate. The characterization techniques presented elsewhere for the 3 samples solidified with spontaneous nucleation were used for the triggered samples [5]. In case of triggering, cooling was achieved with an alumina plate bring into contact with the bottom of the levitating sample.

Modeling

The FE method solves the average conservation equations for energy and solute mass [12, 13] to compute both the average enthalpy, $<H_n>$, and the average composition of solute, $<w_n>$, at each FE node n. The mesh adaptation approach developed by Alauzet and Frey [14] has been implemented. It consists of a minimization method that evaluates the mesh size required to access a given error for a chosen field to be computed using the FE method. The main idea developed by Alauzet and Frey is that the mesh size could be controlled by a directional error estimator based on the recovery of the second derivatives of the finite element solution for a given scalar field. It is known as the Hessian strategy. This directional information is then converted into a mesh metric field which prescribes the desired element size and orientation and hence improves the precision of the FE solution. This strategy was previously successfully applied to the modeling of the welding process [15]. For the present application, the average composition was selected to track the solute field ahead of grains as well as to preserve the segregation pattern in the grain. The Gruau and Coupez [16] unstructured and anisotropic mesh generation technique with adaptation is used to regenerate the FE mesh when required.

A microsegregation model is used to convert the average composition of solute and the average enthalpy of a solid plus liquid mixture into a temperature and a fraction of solid. In the 2D CAFE model, such a conversion is achieved at the scale of the CA cell using interpolations $<H_v>$ and

$<w_\nu>$ at cell ν deduced from values $<H_n>$ and $<w_n>$ at nodes n. Previous considerations were based on the lever rule or Scheil approximation [1, 10, 11, 13]. As demonstrated elsewhere, these approximations are not valid for the Al-Cu system [8, 17]. A modified version of the microsegregation model developed by Wang and Beckermann has consequently been adopted and implemented for each CA cell [7]. For that purpose, the formulation of the average conservation equations for solute mass and total mass in the solid, s, extradendritic liquid, l, and interdendritic liquid, d, proposed in reference 8 have been used. When nucleation temperature is reached at a given cell ν initially in the liquid state, an equilateral quadrilateral surface is defined. The cell is then considered as mushy. This rhombus surface offers a 2D approximation of the grain defined by the primary trunks of the dendritic structure. The growth rate of each half diagonal, **Erreur !** (i=[1, 4]), is calculated as a function of the local supersaturation using the Ivantsov relation [19] together with the marginal stability criteria [20] until it reaches a final value, R_f. The initially equilateral quadrilateral form could not be maintained depending on the solute profile ahead of each tip. The growth rate of the volume fraction of the mushy zone, $\partial g^m{}_{,\nu}/\partial t$, is thus calculated as the mean of a ratio of the geometric surface tips **Erreur !**(i=[1, 4]) to the final position, R_f. For a given mushy cell, the solid volume fraction, $g^s{}_{,\nu}$, temperature, $T^s{}_{,\nu}$, average composition of the solid phase, $<w^s{}_{,\nu}>^s$, and average composition the liquid phase, $<w^l{}_{,\nu}>^l$, are then calculated with respect to $<H_\nu>$ and $<w_\nu>$. The final radius, R_f, is defined as the spatial limit for the growth of each of the rhombus tip, which is of the order of several secondary dendrite arms spacing. Considering the growth of a dendritic grain, this limit can be easily defined as the half of the primary dendrite arms spacing, i.e. $R_f = \lambda_1/2$. While the primary and secondary spacing depend on local solidification parameters and can fluctuate, it is yet assumed constant over the entire system in the present study. In addition, source terms for the mass conservation of solute, $\varphi^{\cdot j}{}_{,\nu}$ {j = s, d and l}, have been added to the model originally proposed by Wang and Beckermann [7] in order to involve the variation of the cell average composition due to solute diffusion, $\partial<w_\nu>/\partial t$. These terms are interpolated based on the variation at the FE nodes, $\partial<w_n>/\partial t$. Back diffusion in the solid phase is neglected at the scale of the FE model. Hence, the cell may only exchange solute either through the interdendritic or the extradendritic liquid phase and thus $\varphi^{\cdot s}{}_{,\nu}$ can be neglected. The relative portions, $\varphi^{\cdot l}{}_{,\nu}$ and $\varphi^{\cdot d}{}_{,\nu}$, can be quantified by introducing an exchange partition ratio, ε_ν, which is defined as $\varphi^{\cdot l}{}_{,\nu} = \varepsilon_\nu \varphi^{\cdot d}{}_{,\nu}$, with $\varepsilon_\nu = g^l{}_{,\nu}/(g^l{}_{,\nu} + g^d{}_{,\nu})$. The average composition of the total liquid phase, f, is calculated as the sum of the average composition of the interdendritic and the extradendritic liquids; i.e. $g^f{}_{,\nu}<w^f{}_{,\nu}>^f = g^d{}_{,\nu}<w^d{}_{,\nu}>^d + g^l{}_{,\nu}<w^l{}_{,\nu}>^l$ where $g^f{}_{,\nu} = g^d{}_{,\nu} + g^l{}_{,\nu}$.

Due to the FE mesh adaptation, the topological link between the FE mesh and the CA grid needs to be recalculating. After a remeshing step, based on the position of its center, C_ν,, each cell ν is assigned a new FE, F, containing C_ν,. Subsequently, the linear interpolation coefficients, $c^{nF}{}_{,\nu}$, are revaluated. Finally, all field computed at the level of the CA grid are reassigned to the FE nodes. This procedure is equivalent to a linear transport of information from the old mesh to the new one with the advantages to give more accuracy and to keep coherence between fields at the two different micro, CA, and macro, FE, scales. Extensive validations of the implementation of the new CAFE model have been conducted considering the growth of a single equiaxed grain using either a uniform temperature model [9] or a one-dimensional numerical model [2, 18].

Results

The grey curves, in Figures 1, are the recorded temperature history for the three Al-Cu samples solidified under EML. Sudden changes of the cooling rates are measured at the time when the alumina plate enters into contact with the sample. This is identified as the nucleation time of the

primary structure, reported in figure 1 as $t_{n,}^{\alpha}$, which correspond to a nucleation undercooling $\Delta T_{N,}^{\alpha}$. Two joint effects coexist after the contact with the trigger. Since nucleation has been initiated using an alumina plate, the cooling rate should first increase due to heat extraction throughout the alumina/droplet contact surface. Fast growth of the structure is then expected, accompanied with latent heat release. These two effects compete and, as is usual in small solidified volumes, can give rise to local reheating. This is observed in Figure 1 within the first second that follows nucleation. Because the nucleation undercooling is larger for the Al-24wt%Cu alloy, dendritic growth is faster and reheating is also larger. A plateau is visible below the eutectic temperature for the Al-24wt%Cu sample. The time and undercooling identified for the nucleation of the eutectic structure are labeled in Figure 1 as $t_{n,}^{E}$ and $\Delta T_{N,}^{E}$. This is not the case for the Al-4wt%Cu samples since the fraction of eutectic is much less. Also labeled in Figure 1 are the end of the solidification, $t_{end,}$, based on the variations of the cooling rate. This information is summarized in Table 1, also for the samples in which spontaneous nucleation was achieved [5]. Other measurements on each curve are the cooling rates just before and after solidification, respectively $\dot{T}_{,}(t<t_{N,}^{\alpha})$ and $\dot{T}_{,}(t>t_{end,})$, listed in Table 1. These cooling rates have been used for the adjustment of the heat transfer coefficient between the sample free surface and the external environment. Two parts of the free surface have been considered. A small cap at the bottom of the spherical domain, $A_1 = 83.75\ 10^{-6}\ m^2$, where the external free surface of the droplet is in contact with the surface of the alumina plate, and the rest of the surface of the 2.65 mm radius spherical sample, $A_2 = 4.5\ 10^{-6}\ m^2$. With an external temperature of 293 K, the fitted values are $h^{A1}(t<t_{N,}^{\alpha})=h^{A2}(t<t_{N,}^{\alpha})=6.4\ W\ m^{-2}\ K^{-1}$ for the Al-4wt%Cu alloy and $h^{A1}(t<t_{N,}^{\alpha})=h^{A2}(t<t_{N,}^{\alpha})=13\ W\ m^{-2}\ K^{-1}$ for the Al-24wt%Cu alloy. For both alloys, the heat transfer coefficient applied on A_2 was unchanged after nucleation, $h^{A2}(t>t_{N,}^{\alpha})=h^{A2}(t<t_{N,}^{\alpha})$, while cooling through the triggering devise used the value $h^{A1}(t>t_{N,}^{\alpha})=10000\ W\ m^{-2}\ K^{-1}$.

Figure 1 present the model prediction of the averaged temperature over the simulation domain, black curves, as well as at the top, ▲,—, and at the bottom of the domain, ▼,—. Sharp changes on the predicted temperature slope at the nucleation point clearly mark the effect of the implemented adjustments of the heat transfer coefficients. A single nucleation event occurs at the bottom of the domain at the measured temperature deduced from the cooling curves and listed in Table 1. The model predicts a large decrease of the temperature after the nucleation of the primary solid phase at the bottom of the system. Contrarily, at the top of the system, an increase of the temperature is predicted; which is due to the latent heat released upon solidification. Due to the important primary phase undercooling for the Al-24wt%Cu sample, $\Delta T_{N,}^{\alpha} = 32$ K, a large amount of latent heat is suddenly released. The liquid at the top of the system is thus reheated leading to a predicted temperature curve that compares favorably with the pyrometer measurement. However, because the measured signal is the result of an average surface temperature seen by the pyrometer, comparison can only remain qualitative.

Additional experimental measurements consist of distribution maps of the copper composition conducted on a meridian cross section of the Al-Cu droplets made through the alumina/droplet surface. 2D SEM image analyses have also been applied to calculate the volume fraction of eutectic and the DAS for the same cross sections [5]. Global averaging over the entire measurements for each sample leads to the values listed in Table 2. These are the average copper composition, w_D, the dendrite arm spacing, DAS_D, and the volume fraction of eutectic, $g_{D,}^{E}$. Results are shown in Figure 2. The average copper content, w_D, shows a deviation from the nominal composition, w_0, that varies from -8.37% for the 24 wt% Cu to +9.25% for the 4 wt% Cu. These deviations are expected to result from a non-symmetric growth of the dendritic

structure with respect to the central meridian cross sections analyzed. Values in Table 2 also show that the average eutectic volume fraction over the entire cutting plane, $g_{D,}^{E}$, are close to the Gulliver-Scheil model prediction, $g_{GS,}^{E}$, for the triggered samples. Deviation from $g_{GS,}^{E}$ are proportionally larger for the Al-Cu samples processed upon EML when nucleation happened spontaneously. In Al-Cu, this is explained by the short solidification times for the triggered samples [5]. A eutectic plateau is also predicted for the Al-24wt%Cu sample in Figure 1. It should be pointed out that, for the Al-24wt%Cu system, eutectic transformation is simulated to start at the measured nucleation temperature, $T_{N,}^{E}=T_{E,}-\Delta T_{N,}^{E}$, leading to the value $g_{CA,}^{E}$ = 65%, very close to what has been measured. This agreement was not reached when the simulation was run with a eutectic transformation starting at the eutectic temperature, $T_{E,}$, given by the phase diagram, leading to a final amount of eutectic equal to $g_{‡,}^{E}$ = 81.4, thus demonstrating the role of the nucleation undercooling of the eutectic microstructure. The present model has also been applied to the EML solidification experiences with spontaneous nucleation [5]. Only the results in terms of the final amount of eutectic are reported in Table 2. The model predictions reported in Table 2, $g_{CA,}^{E}$=6.8% for the Al-4wt%Cu and $g_{CA,}^{E}$=67% for the Al-24wt%Cu and, deviate from the measured value, $g_{D,}^{E}$. These predictions retrieve the results of the simulations presented in reference [5] when an isothermal transformation is assumed to occur at the nucleation undercooling measured for the eutectic structure. The origin of these deviations from the measurements is in fact identified to the eutectic recalescence that is measured for these samples and that can consequently not be neglected [5]. The approximation of an isothermal eutectic transformation is thus identified as a remaining limitation of the present CAFE model. These remarks are of prime importance for quantitative prediction of phase fractions in solidification processes of alloys.

Figure 2 and 3 summarize the experimental and predicted normalized distributions for the average copper composition, w, and the volume fraction of eutectic, $g_{\ ,}^{E}$. The same scales used for the representation of the measured data map are chosen. The magnitude of the segregation is less than the measured one when distribution for each alloy. However, normalization has been achieved using the nominal composition of the sample, 4 and 24 wt% Cu, where the measured copper average content over the cross section are respectively 4.14 and 21.99 wt%. For the triggered Al-4%wt%Cu sample, Figure 2 shows a correlation between the distribution map of copper and the eutectic fraction. This is in line with the distribution maps presented for the spontaneously nucleated samples [5]. Similar trends are observed in the simulated maps presented in Figure 3. Because the eutectic transformation is modeled with no eutectic undercooling, the remaining liquid at $T_{E,}$ that will transform into eutectic only depends on the average local composition and the effect of diffusion in the solid. But the latter effect is small for the triggered samples. Consequently, more eutectic is found in region of lower average copper content, typical of the result know from classical microsegregation analyses. The case of Al-24%wt%Cu is more interesting. There is clearly a deviation from a correlation between the average Cu content and the eutectic fraction at the bottom of the sample, where more eutectic is found for less Cu. This is also predicted and could thus be analyzed into detail. The reason explaining this result is the diffusion of Cu outside the mushy zone that decreases the amount of solute there together with the quenching of the remaining interdendritic liquid into eutectic at the nucleation temperature measured. At the top of the system, more time is available for the dendritic structure to solidify because the cooling rate is smaller as discussed above. Thus less liquid is available for the eutectic transformation.

Summary

- A microsegregation model has been implemented into the 2D CA model together with a FE mesh adaptation technique. The microsegregation model accounts for back diffusion in the solid phase as well as diffusion in the liquid phase using as the primary and secondary dendrite arm spacing as length scale parameters. At the macro-scale, solute and heat diffusion fields in front of the mushy/liquid growth fronts are resolved thanks to the FE solution of the average conservation equations onto a refined FE mesh. Extensive validations of the model have been conducted showing its capability to deal with solute diffusion inside and outside a growing mushy zone [18].
- Considering previous results for spontaneous samples [5] and the above results for triggered samples lead to the conclusion that the effect of solute diffusion in the solid phase, the nucleation temperature of the eutectic structure as well as recalescence due to eutectic growth are the main phenomena to deal with in order to reach quantitative predictions.
- Applications to solidification of Al-Cu droplets processed by EML have been achieved. The predicted temperature histories give access to a comprehensive explanation of the measured cooling curves. Although the predicted distributions of segregation show deviations from the measurements, the model gives similar behaviors and compare favorably with respect to the quantities averaged over the entire volume.
- In view of the above results, more quantitative comparison could certainly be reached with a 3D model including the effect of convection induced by the electromagnetic field as well as the non symmetric behavior of the development of the mushy zone.

Acknowledgements

This work was conducted within a European Space Agency project of the Microgravity Applications Promotion program (contract 15236/02/NL/SH). Contributions from S. Jacomet, B. Triger and M. Repoux are acknowledged. Samples were processed using electromagnetic levitation by Th. Volkmann and D. Herlach at the Deutsches Zentrum für Luft- und Raumfahrt e.V., Köln, Germany.

References

[1] Gandin Ch.-A., Desbiolles J.-L., Rappaz M., Thévoz Ph. Metallurgical and materials transactions A 1999; 30:3153.
[2] Heringer R., Gandin Ch.-A., Lesoult G., Henein H. Acta Materialia 2006; 54:4427.
[3] Herlach D. M. Annual Review of Materials 1991; 21:23.
[4] Kasperovich G., Volkmann T., Ratke L., and Herlach D. Metallurgical Transactions A 2008, 39:1183.
[5] Gandin Ch.-A., Mosbah S., Volkmann Th., Herlach D.M. Acta Materialia 2008; 56:3023.
[6] Mosbah S., Gandin Ch.-A., Brogly J., Crozier B., Volkmann Th., Herlach D. *Solidification Processing*, conference proceedings 2007; 80. Ed. H. Jones. The University of Sheffield, U.K.
[7] Wang C. Y., Beckermann C. Metallurgical Transactions A 1993; 24:2787.
[8] Wang C. Y., Beckermann C. Materials Science and Engineering 1993; 171:199.
[9] Martorano M.A., Beckermann C., Gandin Ch.-A. Metall. mater. trans. 34A (2003) 1657.
[10] Gandin Ch.-A., Rappaz M., Acta metallurgica 1994; 42:2233.
[11] Guillemot G., Gandin Ch. -A., Combeau H. ISIJ International 2006 ; 46:880.

[12] Bellet M., Fachinotti V.D., Gouttebroze S., Liu W., Combeau H. *Solidification Processes and Microstructures: A Symposium in Honor of Prof. W. Kurz* 2004; 15. Eds M. Rappaz, C. Beckermann, R. Trivedi. TMS, Warrendale, PA, U.S.A.
[13] Guillemot G., Gandin Ch. -A., Bellet M. Journal of Crystal Growth 2007; 303:58.
[14] Alauzet F., Frey P.J. INRIA Report 2003; #4759.
[15] Hamide M., Massoni E., Bellet M., Int J. Num Meth. Eng. 2008; 73:624.
[16] Gruau C., Coupez T., Computer Methods Appl. Mech. Engrg. 2005; 194:4951.
[17] Sarreal J. A., Abbaschian G. J. Metallurgical Transactions A 1986; 17:2063.
[18] Mosbah S., Bellet M., Gandin Ch.-A. *Solidification and Gravity 2008*, conference proceedings; in press. Eds. A. Roósz et al. Materials Science Forum, Trans Tech Publications Ltd.
[19] Ivantsov G. P. Doklady Akademii Nauk SSSR 1947; 58:567.
[20] Langer J.S., Müller-Krumbhaar H. J. Cryst. Growth 1977; 42:11.

w_0 [wt%]	Nucleation	$\Delta T_{N,}^{\alpha}$ [°C]	$\Delta T_{N,}^{E}$ [°C]	$\dot{T}, (t<t_{N,}^{\alpha})$ [K s^{-1}]	$\dot{T}, (t>t_{end,})$ [K s^{-1}]	$t_{end,} - t_{N,}^{\alpha}$ [s]
4	triggered	-	-	-1.5	-64	4.2
	spontaneous	35	20	-6.6	-	41.5
24	triggered	32	20	-3.51	-71	5.2
	spontaneous	25	45	-4.5	-	88.2

Table 1: Summary of the measurements deduced from the recorded cooling curves for the three Al-Cu samples processed using electromagnetic levitation. Composition, w_0, cooling rates, $\dot{T}, (t<t_{N,}^{\alpha})$ and $\dot{T}, (t>t_{end,})$, nucleation undercooling of the dendritic and eutectic structures, $\Delta T_{N,}^{\alpha}$ and $\Delta T_{N,}^{E}$, solidification times measured from nucleation of the dendritic structures, $t_{N,}^{\alpha}$, up to completion of the solidification, t_{end}.

w_0 [wt%]	Nucleation	w_D [wt%]	DAS_D [µm]	$g_{D,}^{E}$ [%]	$g_{[5],}^{E}$ [%]	$g_{CA,}^{E}$ [%]	$g_{GS,}^{E}$ [%]
4	triggered	4.37	20	7.91	-	7.36	7.81
	Spontaneous [5]	4.14	30	5.6	5.62	6.8	
24	triggered	21.99	10	61.62	-	65.	67.64
	Spontaneous [5]	20.7	15	57.2	57.5	67.	

Table 2: Summary of measurements deduced from composition measurements (SEM-EDS) and image analyses and present model predictions, $g_{CA,}^{E}$, and Gandin *et al*. [5] model prediction, $g_{[5],}^{E}$.

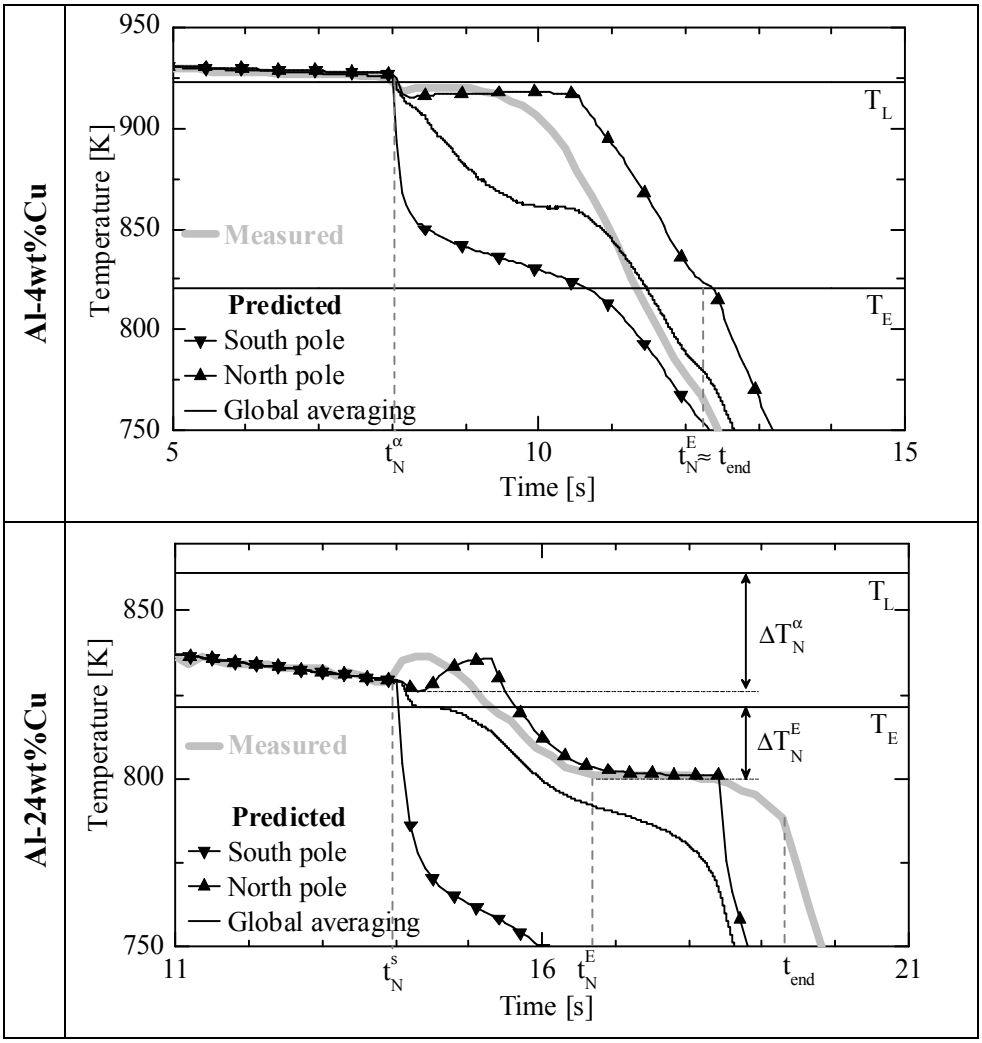

Figure 1: Measured temperature, thick grey curves, for the Al- 4, 14 and 24wt%Cu droplets with initiated nucleation together with the predicted averaged system temperature by the present model, black curves. The predicted temperature at the bottom, ▼,—, and at the top, ▲,—, of the simulation domain are also drawn. Measurements have been achieved using an optical pyrometer at the top of the system. For the Al-24wtCu, nucleation undercooling for the primary solid phase, $\Delta T^{\alpha}{}_{,N}$ = 32 K, as well as for the eutectic structure, $\Delta T^{E}{}_{,N}$ =20 K, have been measured. No undercooling is considered for the Al-4 and 14wt%Cu droplets. Isothermal eutectic transformation is assumed at the measured nucleation temperature for all samples.

Distributions of (top) the normalized average copper content, $(w-w_0)/w_0$, and (bottom) the normalized average volume fraction of eutectic, $(g^E-g_{GS}^E)/g_{GS}^E$, for (left) an Al-4wt%Cu sample and (right) an Al-24wt%Cu sample. Normalization is performed with the nominal alloy composition, w_0, and the volume fraction of eutectic, g^E_{GS}, given by the Gulliver-Scheil approximation (Table

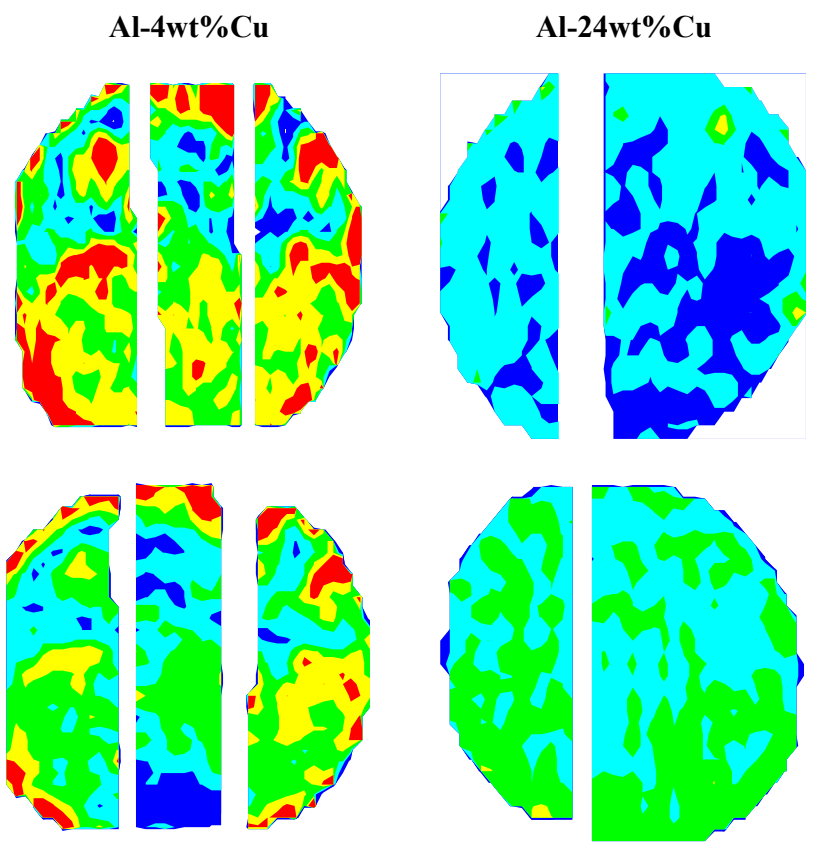

Figure 2. Experimental characterizations within a central meridian cross section of Al-Cu samples processed by electromagnetic levitation with triggered nucleation at the bottom surface.

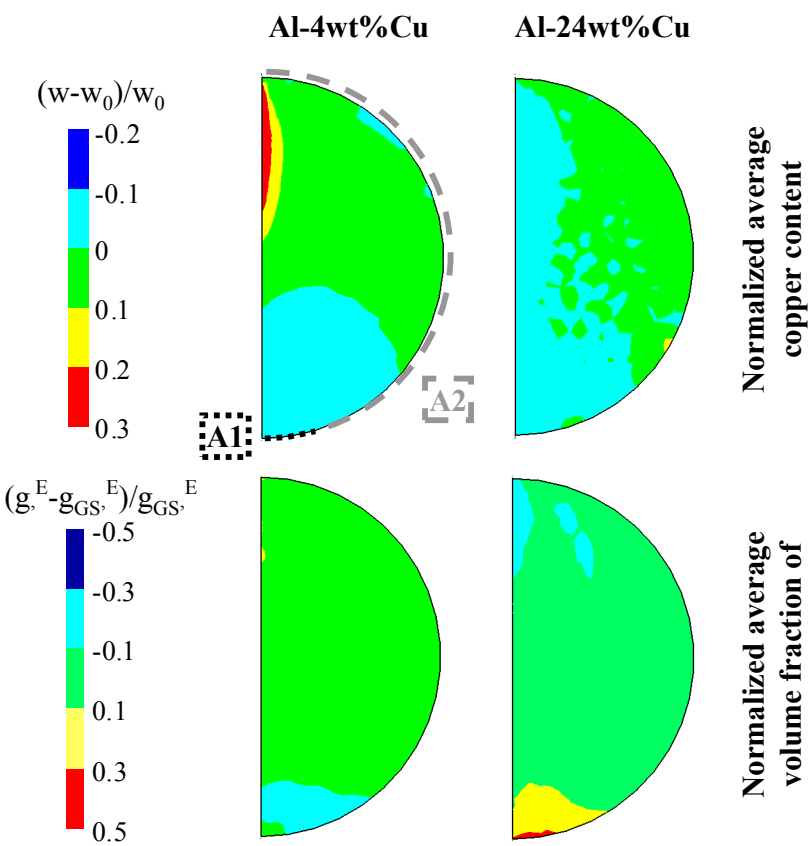

Figure 3: CAFE predictions. Cell size: 10 µm, minimum and maximum FE mesh size: 30 and 200 µm, objective error on the average composition for the FE mesh adaptation: 10^{-4}.